

Asymptotic critical behavior of Ni

M. Seeger, S.N. Kaul,^{*,†} and H. Kronmüller*Institut für Physik, Max-Planck-Institut für Metallforschung, Heisenbergstrasse 1, D-70569 Stuttgart, Germany*

R. Reisser

Max-Planck-Institut für Festkörperforschung, Heisenbergstrasse 1, D-70569 Stuttgart, Germany

(Received 18 August 1994; revised manuscript received 12 January 1995)

The values $\beta = 0.395(10)$, $\gamma = 1.345(10)$, $\delta = 4.35(6)$ for the asymptotic critical exponents, $\mu(0)h_0/k_B T_C = 1.35(10)$, $DJ_0^2/h_0 = 1.20(55)$, $a_M^-/a_\chi^+ = -0.19(6)$ for the universal ratios and the ratio $J_0/J_S(0) = 1.70(16)$, involving asymptotic and correction-to-scaling amplitudes, have been deduced from the bulk magnetic polarization data in the critical region near the ferromagnetic (FM)-paramagnetic (PM) phase transition of polycrystalline Ni samples of different shapes through an elaborate data analysis. These values, though close to those predicted by the renormalization-group calculations for a three-dimensional isotropic short-range Heisenberg ferromagnet, are shifted towards the mean-field estimates. Such a shift is taken to be evidence for a crossover to the fixed point corresponding to isotropic long-range exchange interactions. In accordance with the theoretical expectations, nonanalytic corrections (originating from the nonlinear irrelevant scaling fields) to the singular behavior at T_C (Curie point) dominate over the analytic ones (arising on account of the nonlinear relevant scaling fields) in the critical region but the reverse is true for $T \gg T_C$. Initial susceptibility follows the generalized Curie-Weiss law [Eq. (14) of the text with $\tilde{a}_{\chi_1} = 0$] from T_C to $1.4T_C$ and the Curie constant permits an accurate determination of the atomic moment in the PM state. Not all but only about 80% of the moments (spins) in Ni actually participate in the FM-PM phase transition.

I. INTRODUCTION

The static critical behavior near the ferromagnetic-paramagnetic (FM-PM) phase transition of elemental crystalline ferromagnets such as Fe and Ni has been investigated using widely different experimental techniques by several workers for more than three decades now. However, most of the measurements have been performed in a temperature range which lies well outside the asymptotic critical region [ACR = $|\epsilon = (T - T_C)/T_C| \leq 10^{-2}$] and the values quoted for the critical exponents α , β , and γ for specific heat, spontaneous magnetic polarization (J_S), and initial susceptibility (χ_0), respectively, vary by as much as¹ 20% in Fe and Ni. Even in those cases where the Curie temperature (T_C) was approached closer than $\epsilon = 10^{-2}$, the data have been fitted to a *single power* law over a wide range of temperatures in the vicinity of T_C and such a data analysis yields an *effective* critical exponent whose value depends on the temperature range chosen for the fit. The reported values of the *effective* critical exponents significantly differ² from the renormalization-group (RG) estimates³ for the *asymptotic* critical exponents that characterize the leading singular behavior at the critical point in materials, belonging to the universality class (n = order parameter dimensionality = 3, d = space dimensionality = 3), such as Fe and Ni. These deviations are generally attributed² to the complications arising from the presence of dipolar long-range interactions. A similar discrepancy between experimental results and theoretical predictions has been

reported⁴ in the past in the case of amorphous ferromagnets as well. However, subsequently an elaborate data analysis,⁵⁻⁸ which takes into account the leading confluent singularity terms (originating from the irrelevant scaling fields) predicted by the RG theories,^{9,10} revealed that for amorphous ferromagnets the deviations in question are an artifact of the single-power-law analysis, which completely ignores the correction-to-scaling (CTS) terms. In view of this development, a definite conclusion about the genuineness of the deviations in crystalline ferromagnets can be drawn only when the true asymptotic critical exponents for these materials are determined experimentally. Moreover, a rigorous test for the RG predictions concerning the static critical behavior of pure isotropic three-dimensional (3D) Heisenberg systems or about the crossover effects in the presence of dipolar interactions is not possible unless the experimental values are available not only for the asymptotic critical exponents but also for the universal amplitude ratios. This prompted us to accurately determine the values of asymptotic (leading CTS) critical exponents β and γ and critical amplitudes (amplitudes) for Ni from high-precision bulk magnetic polarization (BMP) data taken in the asymptotic critical region.

Another motivating factor for undertaking BMP measurements in the ACR was to seek an answer to the following basic question. What is the effect of shape anisotropy on the low-field deviations from the linear modified Arrott plot isotherms usually encountered in crystalline and amorphous ferromagnets?

II. EXPERIMENTAL DETAILS

Ni rods of 99.99% purity were cast into the cylindrical shape (diameter ≈ 9 mm) after melting them in the electron beam furnace. The cylindrical ingots, so obtained, were annealed at 850 °C for 6 days under a hydrogen atmosphere and subsequently degassed at 800 °C for 12 h. Samples of four different shapes, i.e., a *sphere* of 5 mm diameter (sample No. 1), a *disk* of 5 mm diameter and 0.5 mm thickness (sample No. 2), a *square slab* of dimensions $5 \times 5 \times 0.5$ mm³ (sample No. 3), and a *cube* of dimensions $5 \times 5 \times 5$ mm³ (sample No. 4), were spark cut from the cylindrical ingots. Surface contamination, if any, was removed in sample No. 1 by chemical etching in a solution of ethanol and bromine and in the remaining samples by mechanical polishing. All the samples were annealed at 800 °C for 1 day under high vacuum ($\approx 10^{-6}$ Torr) to relieve surface stresses.

Magnetic polarization was measured in external magnetic fields up to 0.9 T at fixed temperatures (stable to within ± 40 mK), ≈ 0.5 K apart in the critical region and about 5 K apart for temperatures far away from T_C , over a wide range $0.9T_C \leq T \leq 1.4T_C$ using a vibrating sample magnetometer (EG&G PAR 150A). Sample temperature was monitored by a precalibrated NiCr-NiAl thermocouple in direct contact with the sample and controlled by a proportional, integral, and differential temperature controller. The demagnetization factor N for each sample was determined from the low-field (≤ 10 mT) magnetic polarization data and the values of N for sample Nos. 1, 2, 3, and 4 are 0.32, 0.086, 0.07, and 0.271, respectively. The external field $\mu_0 H_{\text{ext}}$ was corrected for the demagnetizing field NJ to arrive at the values of the internal field.

III. RESULTS AND DATA ANALYSIS

Figure 1 shows a typical modified Arrott [$J^{1/\beta_{\text{eff}}}$ versus $(\mu_0 H/J)^{1/\gamma_{\text{eff}}}$] plot constructed out of the “raw” magnetic polarization $J(\mu_0 H_{\text{ext}}, T)$ data by varying the effective critical exponents β_{eff} and γ_{eff} until $J^{1/\beta_{\text{eff}}}$ versus $(\mu_0 H/J)^{1/\gamma_{\text{eff}}}$ isotherms in a narrow temperature range

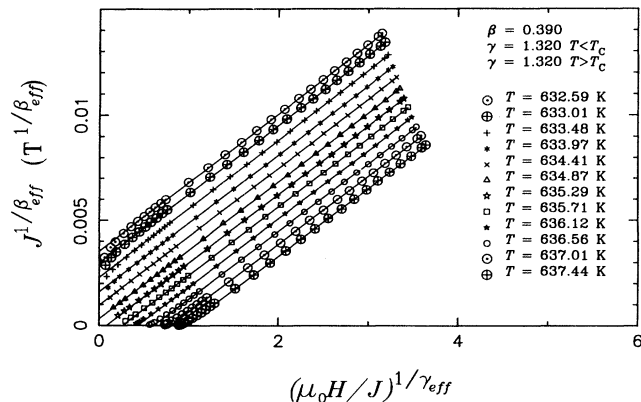


FIG. 1. Modified Arrott plot for polycrystalline Ni sample No. 3.

around T_C are straight and parallel to one another over as wide a range of $(\mu_0 H/J)$ values as possible. In such plots, the internal field $\mu_0 H$ is obtained by subtracting the demagnetizing field NJ from the external magnetic field $\mu_0 H_{\text{ext}}$. The deviations at low fields from the linear modified Arrott plot isotherms (Fig. 1) look exactly the same for Ni samples of different shape (sample Nos. 1–4) and hence we conclude that the shape anisotropy does not have any significant effect on these deviations. The spontaneous magnetic polarization $J_S(T)$ and inverse initial susceptibility $\chi_0^{-1}(T)$ at different temperatures are then computed from the intercepts on the $J^{1/\beta_{\text{eff}}}$ (for $T < T_C$) and $(\mu_0 H/J)^{1/\gamma_{\text{eff}}}$ (for $T > T_C$) axes obtained by a linear extrapolation,^{4–8,11–15} as shown in Fig. 1, of the high-field linear portions of the modified Arrott plot isotherms to $(\mu_0 H/J)^{1/\gamma_{\text{eff}}} = 0$ and $J^{1/\beta_{\text{eff}}} = 0$. The $J_S(T)$ and $\chi_0^{-1}(T)$ data for all the four samples of polycrystalline Ni, extracted from the modified Arrott plots in this way, are compared in Figs. 2 and 3. It is noticed from these figures that the overall temperature dependence and even the absolute magnitudes of J_S and χ_0^{-1} at any specified value of reduced temperature ϵ are nearly the same for the different sets of data. In view of such a close agreement, illustrative plots for only one sample, namely, sample No. 3, are shown in the greater part of this paper.

A. Single-power-law analysis

At first, we follow the customary approach of fitting the single power laws, e.g.,

$$J_S(T) = J_0^{\text{eff}} (-\epsilon)^{\beta_{\text{eff}}}, \quad \epsilon < 0, \quad (1)$$

and

$$\chi_0^{-1}(T) = (h_0/J_0)^{\text{eff}} \epsilon^{\gamma_{\text{eff}}}, \quad \epsilon > 0, \quad (2)$$

where J_0^{eff} and $(h_0/J_0)^{\text{eff}}$ are the effective critical amplitudes, to the $J_S(T)$ and $\chi_0^{-1}(T)$ data taken at temperatures in the immediate vicinity of T_C .

Agreement of the theoretical fits, based on Eqs. (1) and (2), with the experimental data is optimized by vary-

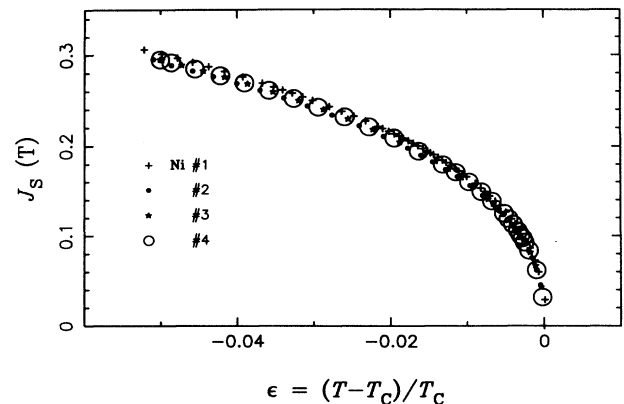


FIG. 2. Temperature variation of spontaneous magnetic polarization for all the Ni samples.

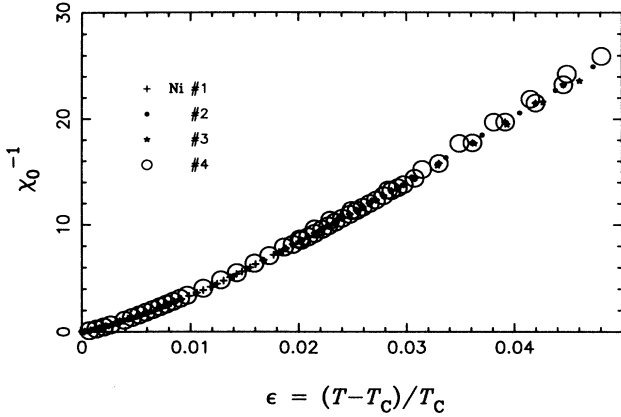


FIG. 3. Temperature dependence of inverse initial susceptibility for all the Ni samples.

ing the effective critical exponents and amplitudes as well as T_C . The best least-squares fits in the specified temperature ranges are obtained for the choice of the parameters given in Tables I and II. We have cross-checked the parameter values listed in Tables I and II by following the celebrated Kouvel-Fisher (KF) approach,¹⁶ which makes use of the alternative form of Eqs. (1) and (2), i.e.,

$$Y(T) = J_S(T) |dJ_S(T)/dT|^{-1} = |(T - T_C)|/\beta_{\text{eff}} = (T_C/\beta_{\text{eff}})|\epsilon|, \quad \epsilon < 0, \quad (3)$$

and

$$X(T) = \chi_0^{-1}(T) [d\chi_0^{-1}(T)/dT]^{-1} = (T - T_C)/\gamma_{\text{eff}} = (T_C/\gamma_{\text{eff}})\epsilon, \quad \epsilon > 0, \quad (4)$$

and whose details are given elsewhere.^{4-8,11-15} The plots of the quantities Y and X against ϵ , displayed in Fig. 4, clearly demonstrate the validity of Eqs. (3) and (4) [hence of Eqs. (1) and (2)] in a narrow temperature interval around T_C . Moreover, the least-squares fits to the

$Y(T)$ and $X(T)$ data (straight lines in Fig. 4) in temperature ranges the same as above, based on Eqs. (3) and (4), yield exactly the same values for β_{eff} , γ_{eff} (inverse slope) and T_C^- , T_C^+ (intercept on the T axis) as those given in Tables I and II. The above analysis is henceforth referred to as the KF analysis.

B. Analysis with confluent singularity terms

Next, the $J_S(T)$ and $\chi_0^{-1}(T)$ data are analyzed in terms of the expressions

$$J_S(T) = J_0(-\epsilon)^\beta [1 + a_M^-(-\epsilon)^\Delta], \quad \epsilon < 0, \quad (5)$$

and

$$\chi_0^{-1}(T) = (h_0/J_0)\epsilon^\gamma [1 + a_X^+\epsilon^\Delta]^{-1}, \quad \epsilon > 0, \quad (6)$$

which take into account the leading nonanalytic correction-to-scaling (CTS) term¹⁷ arising from the irrelevant scaling fields, as predicted by the RG calculations.^{9,10} In this analysis (the so-called CTS analysis), theoretical fits to the data are attempted based on Eqs. (5) and (6) with the aid of a nonlinear least-squares fitting computer program which varies the fitting parameters J_0 [h_0/J_0], T_C^- [T_C^+], β [γ], and a_M^- [a_X^+] but keeps Δ constant at its theoretically predicted³ value for 3D Heisenberg systems, i.e., $\Delta = 0.55$, to optimize agreement with the experimental $J_S(T)$ [$\chi_0^{-1}(T)$] data. The optimal values of the fitting parameters listed in Tables I and II are arrived at by using a range-of-fit analysis in which the variation of these parameters is monitored as the fit range $|\epsilon_{\min}| \leq |\epsilon| \leq |\epsilon_{\max}|$ is narrowed down by lowering $|\epsilon_{\max}|$ towards $|\epsilon_{\min}|$, which is kept fixed. The width of the ACR is given by the temperature range (see Tables I and II) over which the fitting parameters possess stable (to within the uncertainty limits given in Tables I and II) values, i.e., the optimal values mentioned above. By contrast, the range-of-fit analysis which

TABLE I. Fit parameters for the spontaneous magnetic polarization J_S of polycrystalline Ni. Abbreviations: CTS, correction-to-scaling; KF, Kouvel-Fisher.

Sample No.	Analysis	Fit range		T_C^- (K)	β	J_0 (T)	a_M^-
		$ \epsilon_{\min} $	$ \epsilon_{\max} $				
1	CTS	6.8×10^{-4}	8.0×10^{-2}	635.53(2)	0.395(10)	1.04(7)	-0.39(5)
	KF	6.1×10^{-4}	6.3×10^{-3}	635.49(6)	0.379(11)	0.95(7)	
2	CTS	4.4×10^{-4}	5.1×10^{-2}	634.72(2)	0.405(10)	1.10(6)	-0.40(5)
	KF	3.8×10^{-4}	5.2×10^{-3}	634.68(5)	0.390(10)	0.96(7)	
3	CTS	3.6×10^{-4}	5.0×10^{-2}	635.09(1)	0.392(10)	1.04(4)	-0.35(5)
	KF	3.6×10^{-4}	5.8×10^{-3}	635.09(4)	0.391(10)	0.97(7)	
4	CTS	1.7×10^{-4}	5.0×10^{-2}	634.28(2)	0.405(10)	1.10(7)	-0.45(5)
	KF	9.1×10^{-5}	6.7×10^{-3}	634.22(5)	0.392(12)	0.99(7)	

TABLE II. Fit parameters for the initial susceptibility χ_0^{-1} of polycrystalline Ni. Abbreviations: CTS, correction-to-scaling; KF, Kouvel-Fisher.

Sample No.	Analysis	Fit range		T_C^+ (K)	γ	$\frac{h_0}{J_0}$	a_χ^+
		$ \epsilon_{\min} $	$ \epsilon_{\max} $				
1	CTS	2.4×10^{-4}	1.2×10^{-2}	635.54(2)	1.345(10)	2050(70)	2.0(3)
	KF	2.4×10^{-4}	4.2×10^{-3}	635.54(6)	1.314(16)	1681(217)	
2	CTS	4.7×10^{-4}	1.8×10^{-2}	634.65(2)	1.350(10)	1960(50)	1.7(3)
	KF	4.8×10^{-4}	5.0×10^{-3}	634.66(4)	1.300(15)	1363(143)	
3	CTS	3.0×10^{-4}	1.4×10^{-2}	635.09(1)	1.340(10)	1986(60)	2.5(2)
	KF	3.4×10^{-4}	3.0×10^{-3}	635.08(4)	1.314(16)	1523(150)	
4	CTS	6.5×10^{-4}	1.7×10^{-2}	634.27(2)	1.340(10)	1970(80)	2.1(3)
	KF	7.6×10^{-4}	6.4×10^{-3}	634.22(5)	1.315(15)	1531(158)	

makes use of the single power laws [Eqs. (1) and (2)] reveals that all the parameters, i.e., the Curie temperature, *effective* critical exponents, and amplitudes, in the KF fits *depend* on the temperature range chosen for the fit; however, only in the limit $|\epsilon| \rightarrow 0$ do they assume constant values. Furthermore, the CTS fits (denoted in Figs. 5 and 6 by the solid curves) are far *superior* to the KF fits when compared in the same temperature range, as inferred from the substantially reduced value of the sum of deviation squares, χ^2 , in the former type of fits compared to that in the latter. The superiority of the CTS fits [and hence the need to include the CTS terms in the expressions for $J_S(T)$ and $\chi_0^{-1}(T)$] is made all the more obvious by the deviation plots (i.e., the plots of $\Delta J_S/J_S = [J_S(\text{expt}) - J_S(\text{calc})]/J_S(\text{expt})$ and $\Delta \chi_0^{-1}/\chi_0^{-1} = [\chi_0^{-1}(\text{expt}) - \chi_0^{-1}(\text{calc})]/\chi_0^{-1}(\text{expt})$ against $|\epsilon|$) shown in Figs. 7 and 8. From these figures, which depict the percentage deviation of the data from the best KF or CTS fit as a function of reduced temperature, it is evident that the CTS fits closely reproduce the variations

of J_S and χ_0^{-1} with temperature over a wide temperature range whereas the KF fits present systematic deviations from the actual data in the entire temperature range covered in the fits.

A rigorous test for the accuracy of the parameter values yielded by the CTS analysis is provided by the following consistency criterion. In view of the relations^{5-8,10}

$$\beta_{\text{eff}}(\epsilon) = d[\ln J_S(\epsilon)]/d(\ln |\epsilon|) = \beta + a_M^- \Delta |\epsilon|^\Delta \quad (7)$$

and

$$\gamma_{\text{eff}}(\epsilon) = d[\ln \chi_0^{-1}(\epsilon)]/d(\ln \epsilon) = \gamma - a_\chi^+ \Delta |\epsilon|^\Delta, \quad (8)$$

which exist between the *effective* and *asymptotic* critical exponents for $J_S(T)$ and $\chi_0^{-1}(T)$ for temperatures in the close proximity to T_C , the CTS values of β (γ) and a_M^- (a_χ^+), given in Tables I and II, when used in Eqs. (7) and (8) with Δ fixed at the value 0.55, should reproduce the observed variation of β_{eff} (γ_{eff}) with ϵ deduced from the alternative form of Eqs. (3) and (4), i.e.,

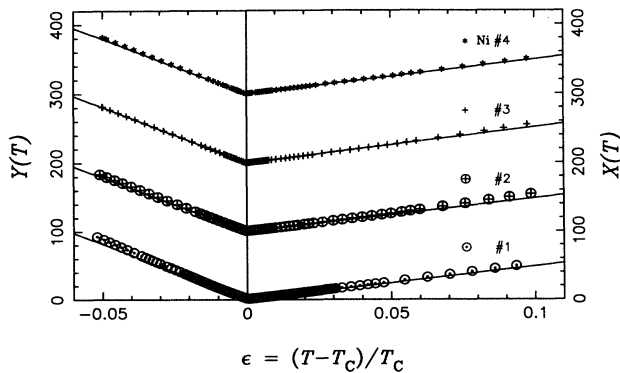


FIG. 4. The quantities $X(T)$ and $Y(T)$ as functions of the reduced temperature. The KF fits based on Eqs. (3) and (4) of the text with the choice of parameters given in Tables I and II are shown as straight lines through the data points. Note the shift of origin on the ordinate axis.

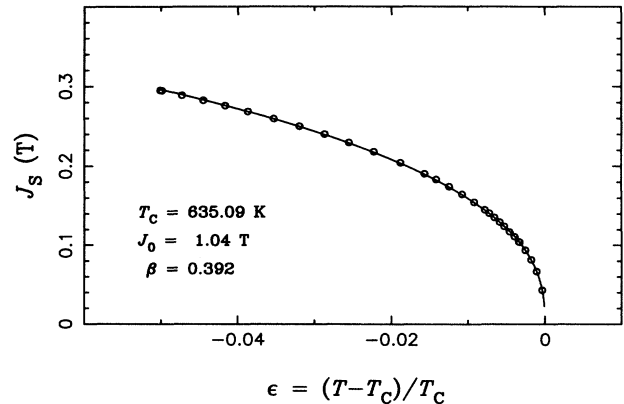


FIG. 5. Temperature dependence of spontaneous magnetic polarization for the Ni sample No. 3 in the asymptotic critical region. The solid curve through the data points represents the CTS fit based on Eq. (5).

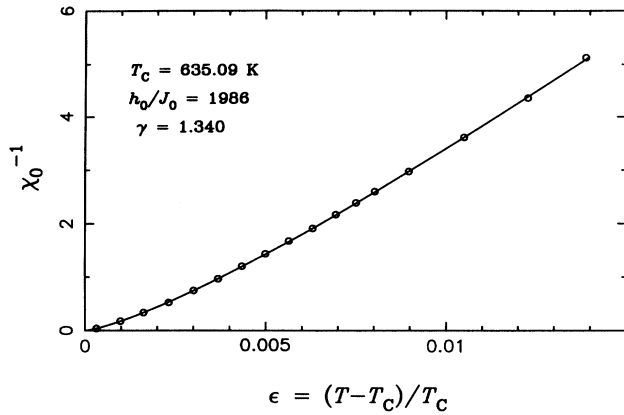


FIG. 6. Temperature variation of inverse initial susceptibility for the Ni sample No. 3 in the asymptotic critical region. The solid curve through the data points depicts the CTS fit based on Eq. (6).

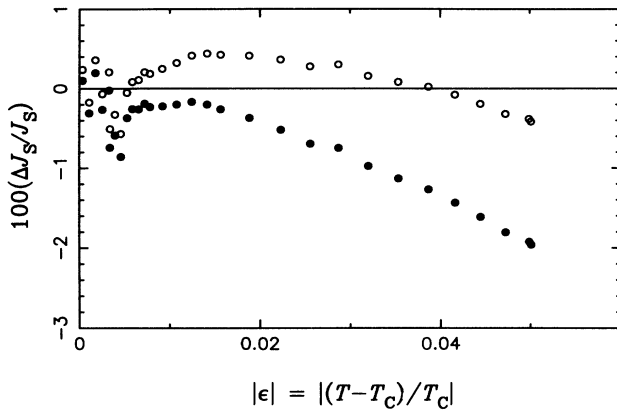


FIG. 7. Percentage deviation of the $J_S(\epsilon)$ data for the Ni sample No. 3 from the KF (solid circles) and CTS (open circles) least-squares fits, based on Eqs. (1) and (5), respectively.

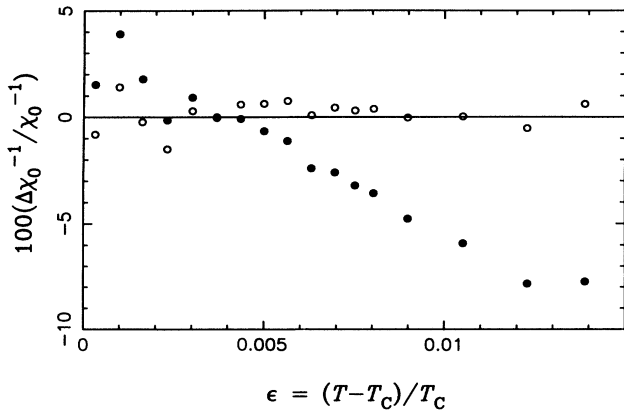


FIG. 8. Percentage deviation of the $\chi_0^{-1}(\epsilon)$ data for the Ni sample No. 3 from the KF (solid circles) and CTS (open circles) least-squares fits, based on Eqs. (2) and (6), respectively.

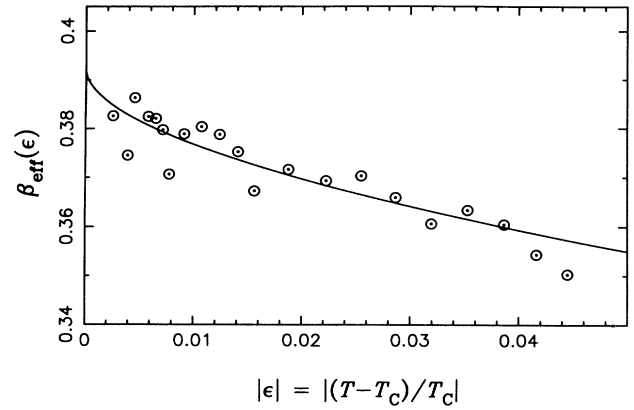


FIG. 9. Temperature dependence of the *effective* critical exponent for spontaneous magnetic polarization of the Ni sample No. 3. The solid curve through the data points depicts the theoretical variation predicted by Eq. (7) with the parameter values given in Table I.

$$\beta_{\text{eff}}(\epsilon) = |(T - T_C)|/Y(T) = [T_C/Y(T)]|\epsilon|, \quad \epsilon < 0, \quad (9)$$

and

$$\gamma_{\text{eff}}(\epsilon) = (T - T_C)/X(T) = [T_C/X(T)]\epsilon, \quad \epsilon > 0. \quad (10)$$

That this is indeed the case is demonstrated by Figs. 9 and 10 wherein the $\beta_{\text{eff}}(\epsilon)$ and $\gamma_{\text{eff}}(\epsilon)$ data (open circles), deduced from Eqs. (9) and (10) using the KF value of T_C (which is the same as that obtained from the CTS analysis; see Tables I and II) and experimental values of $Y(T)$ and $X(T)$, are compared with the theoretical temperature dependence of β_{eff} and γ_{eff} (solid curves) predicted by Eqs. (7) and (8) with the CTS values for β , a_M^- and γ , a_χ^+ , respectively. Note that the scatter in the $\beta_{\text{eff}}(\epsilon)$ and $\gamma_{\text{eff}}(\epsilon)$ data is partly due to the uncertainty in T_C (particularly for the data points close to $\epsilon = 0$) and partly because the three-point differentiation method has been

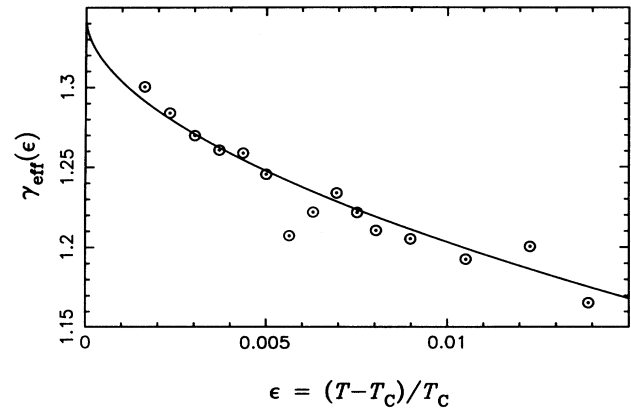


FIG. 10. Temperature variation of the *effective* critical exponent for initial susceptibility of the Ni sample No. 3. The solid curve through the data points depicts the theoretical variation predicted by Eq. (8) with the parameter values given in Table II.

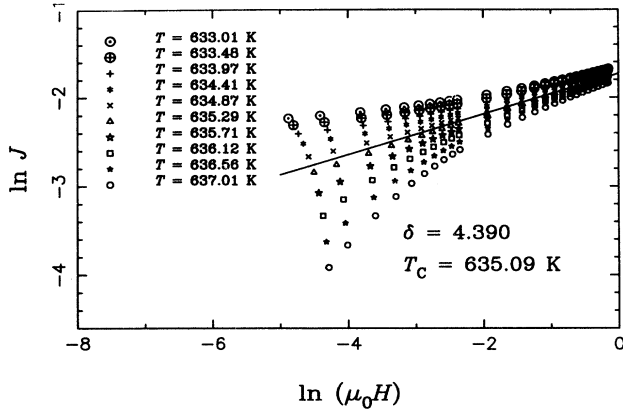


FIG. 11. The $\ln J$ versus $\ln(\mu_0 H)$ isotherms at a few temperatures around the Curie temperature T_C for the Ni sample No. 3. The straight line represents the best least-squares fit to the critical isotherm based on Eq. (11) of the text.

used to compute the quantities $Y(T)$ and $X(T)$ from the $J_S(T)$ and $\chi_0^{-1}(T)$ data. Had the CTS term not been significant, β_{eff} and γ_{eff} would have possessed constant values in the temperature ranges covered in Figs. 9 and 10, an inference in direct contradiction with the observation. Thus, the importance of the CTS terms in the ACR cannot be overlooked.

In order to determine the critical exponent δ for the magnetic polarization versus field isotherm taken at $T = T_C$, we make use of the definition

$$J = A_0(\mu_0 H)^{1/\delta}, \quad \epsilon = 0, \quad (11)$$

TABLE III. Comparison between experiment and theory. Abbreviations: ($d = 3, n = 1$) = 3D Ising model, ($d = 3, n = 3$) = 3D Heisenberg model, MFT = molecular field theory, PW = present work, the numbers 1, 2, 3, and 4 denote the sample numbers.

Parameters	Experiment				Ref. 18	Ref. 19	Theory ^a		
	PW 1	PW 2	PW 3	PW 4			($d = 3, n = 1$)	($d = 3, n = 3$)	MFT
β	0.395(10)	0.405(10)	0.392(10)	0.405(10)		0.390(4)	0.325(2)	0.365(3)	0.5
β_{eff}	0.379(11)	0.390(10)	0.391(10)	0.392(12)	0.378(4)				
γ	1.345(10)	1.350(10)	1.340(10)	1.340(10)			1.241(2)	1.386(4)	1.0
γ_{eff}	1.314(16)	1.300(15)	1.314(16)	1.315(15)	1.34(1)	1.315(15)			
δ	4.52(2)	4.35(2)	4.39(2)	4.31(2)	4.58(5)		4.82(2)	4.80(4)	3.0
$\beta\delta$	1.785(54)	1.762(52)	1.721(52)	1.746(73)			1.567(17)	1.752(29)	1.5
$\beta + \gamma$	1.740(20)	1.755(20)	1.732(20)	1.745(25)			1.565(5)	1.751(7)	1.5
$\beta_{\text{eff}}\delta$	1.713(59)	1.697(52)	1.716(52)	1.690(59)	1.731				
$\beta_{\text{eff}} + \gamma_{\text{eff}}$	1.693(27)	1.690(25)	1.705(26)	1.707(27)	1.718				
$J_S(0)$ (T)	0.635	0.635	0.635	0.635	0.656				
$J_0/J_S(0)$	1.64(12)	1.73(11)	1.64(7)	1.73(11)		1.52(2)	1.486(1)	1.37(7)	1.732
$J_0^{\text{eff}}/J_S(0)$	1.50(12)	1.51(12)	1.53(12)	1.56(12)	1.422				
$\mu(0)$ (μ_B)	0.60	0.60	0.60	0.60	0.616				
$\mu(0)h_0/k_B T_C$	1.35(10)	1.37(11)	1.31(10)	1.38(10)			1.52	1.58	1.732
$\mu(0)h_0^{\text{eff}}/k_B T_C$	1.02(20)	0.83(15)	0.94(19)	0.97(17)	1.037				
D ($\text{T}^{1-\delta}$)	2398(53)	1844(55)	1810(45)	1721(50)					
DJ_0^{δ}/h_0	1.34(60)	1.29(46)	1.04(29)	1.20(46)		1.8(5)	1.81	1.33(1)	1.0
$D(J_0^{\text{eff}})^{\delta}/h_0^{\text{eff}}$	1.19(71)	1.18(66)	1.07(63)	1.10(58)	1.32				

^aReferences 3, 4, and 20.

and construct $\ln J$ versus $\ln(\mu_0 H)$ plots for temperatures near T_C , as illustrated in Fig. 11. According to Eq. (11), a plot of $\ln J$ against $\ln(\mu_0 H)$ should be a straight line with slope δ^{-1} and intercept on the ordinate equal to $\ln A_0$ for the critical isotherm $J(\mu_0 H, T = T_C)$. It is evident from Fig. 11 that the isotherm at $T = T_C$ is indeed a straight line whereas the isotherms taken at $T \neq T_C$ exhibit a concave-upward and concave-downward curvature for $T < T_C$ and $T > T_C$, respectively. The values of the critical amplitude $D (= A_0^{\delta})$ and exponent δ for different Ni samples are listed in Table III.

IV. DISCUSSION

The presently determined values of the asymptotic and effective critical exponents and of the *universal* and effective critical amplitude ratios are compared in Table III with the experimental values for some of these quantities reported^{18,19} earlier and the numerical estimates yielded by the RG calculations^{3,4,20} for 3D Ising and Heisenberg spin systems and by the molecular field theory⁴ (MFT). The important points that emerge from this comparison are as follows. (i) Out of all theoretical values of the asymptotic critical exponents, only those predicted for a 3D isotropic short-range Heisenberg ferromagnet deviate the least from our values, which present a *systematic shift* towards the mean-field (MF) estimates. (ii) Consistent with this shift, the ratio $J_0/J_S(0)$ possesses a value close to that predicted by the MFT. (iii) While the present value of the universal amplitude ratio DJ_0^{δ}/h_0 cannot distinguish between the predictions of different theoretical models due to the large uncertainty, the ra-

tio $\mu(0)h_0/k_B T_C$ has a value which is lower than that given by the theory. (iv) The Widom scaling relation $\beta\delta = \beta + \gamma$ is obeyed and the experimental value of the gap exponent $\Delta = \beta + \gamma$ conforms very well with the 3D Heisenberg value. (v) Our values for the effective critical exponents are in excellent agreement with those determined earlier^{18,19,21–24} by the same and/or other techniques in similar reduced temperature ranges. Similarly, our best estimates (corresponding to the data sets that yield the most stable values for the parameters in the range-of-fit analysis) for the asymptotic critical exponents [$\beta = 0.395(10)$ and $\gamma = 1.345(10)$], universal amplitude ratios [$\mu(0)h_0/k_B T_C = 1.35(10)$ and $DJ_0^\delta/h_0 = 1.20(55)$], ratio [$J_0/J_S(0) = 1.70(16)$], and the correction-to-scaling amplitudes [$a_M^- = -0.40(5)$ and $a_\chi^+ = 2.1(4)$] are in close conformity with those¹⁹ [$\beta = 0.390(4)$, $J_0/J_S(0) = 1.52(2)$, $DJ_0^\delta/h_0 = 1.8(5)$, and $a_M^- = -0.42(4)$] deduced from the neutron depolarization measurements.

As already mentioned in the Introduction (Sec. I), it is customary to attribute^{1,2} the systematic shift observed previously^{1,2,15,16,18,21–24} in the values of effective critical exponents towards the MF values to the presence of isotropic dipolar long-range (IDL) interactions. RG calculations^{25–29} on ferromagnetic systems in which IDL interactions exist in association with isotropic short-range (ISR) Heisenberg exchange interactions have revealed that (a) ISR 3D Heisenberg fixed point is *unstable*²⁵ against IDL perturbations and as the temperature is lowered towards the critical point T_C , from $T \gg T_C$, a *crossover* from the ISR 3D Heisenberg-like critical behavior ($\epsilon \gg \epsilon_{co}$) to the IDL fixed point ($\epsilon \ll \epsilon_{co}$) occurs at a temperature $\epsilon_{co} = g^{1/\phi}$, where the dimensionless parameter g is a measure of the strength of the dipolar perturbation relative to the exchange energy and the *crossover exponent* ϕ equals^{25,26} the ISR 3D Heisenberg susceptibility exponent γ_H , (b) the values of asymptotic critical exponents, characterizing the IDL fixed point, are very close²⁷ (to within 0.5%) to their ISR 3D Heisenberg counterparts but shifted *away* from the MF values, and (c) as a consequence of the ISR-IDL crossover, the *effective* susceptibility exponent, defined by Eq. (8), as a function of reduced temperature, i.e., $\gamma_{eff}(\epsilon)$, goes through a *minimum*²⁸ (dip) [which is *universal*²⁹ for weak ($g \approx 10^{-6}$) dipolar ferromagnets only] at a temperature $\epsilon_{dip} \approx g \tilde{\epsilon}_{dip} = g|[T - T_C(g)]/[T_C(g) - T_C(0)]|_{dip}$, where $T_C(0)$ [$T_C(g)$] denotes the critical temperature for the system with ISR Heisenberg exchange interactions only [ISR Heisenberg plus IDL interactions]. The numerical estimates $g = 3.2 \times 10^{-5}$, $\phi = \gamma_H = 1.37$, and $\tilde{\epsilon}_{dip} \approx 1.8$ given in Refs. 26–28 yield the values for ϵ_{co} and ϵ_{dip} for Ni as $\epsilon_{co} = 5.2 \times 10^{-4}$ and $\epsilon_{dip} \approx 5.8 \times 10^{-5}$. Considering that the temperature range, which marks the critical region above T_C in the present experiments (typically $5.0 \times 10^{-4} \leq \epsilon \leq 1.5 \times 10^{-2}$; see Table II), lies above ϵ_{co} and ϵ_{dip} , the RG predictions (a)–(c) stated above assert that in the temperature range in question Ni should exhibit a critical behavior associated with the ISR 3D Heisenberg fixed point and $\gamma_{eff}(\epsilon)$ should *increase* with increasing ϵ . Though the critical exponents possess ISR 3D Heisenberg-like values, γ_{eff} *decreases* with increasing

ϵ (Fig. 10). The latter observation, made previously^{15,16} by other workers too, is in *direct contradiction* with the RG prediction (c). By contrast, a shallow minimum in $\gamma_{eff}(\epsilon)$ at the theoretically predicted²⁸ value of ϵ_{dip} has indeed been observed³⁰ in an isotropic Heisenberg ferromagnet with appreciable isotropic dipolar interactions such as EuO for which²⁶ $g = 1.7 \times 10^{-2}$. The other extreme case is represented by antiferromagnets in which IDL interactions, if present, are expected to be *irrelevant*²⁵ in the RG sense. Consistent with this theoretical expectation, the *nonmonotonic*²⁸ variation of the effective specific heat exponent with ϵ in the IDL-ISR crossover region is completely absent³¹ in a 3D ISR Heisenberg antiferromagnet such as RbMnF₃.

A possible explanation for the discrepancy between theory and experiment in the present case could be sought in an incorrect estimate of ϵ_{co} and ϵ_{dip} for Ni; i.e., if one imagines that the observed variation of γ_{eff} with ϵ actually represents the theoretical $\gamma_{eff}(\epsilon)$ for $\epsilon < \epsilon_{dip}$, ϵ_{co} , the parameter g should have a value which is *three orders of magnitude higher* than that previously assumed. In view of the perfect agreement between the theoretically predicted and experimentally observed variations of the effective critical exponents with ϵ in the crossover region in the other two cases mentioned above and the fact that a value of g as high as 3.2×10^{-2} (that is, close those²⁶ for ferromagnets such as EuO and EuS in which IDL interactions are known to be comparable in strength to ISR exchange interactions) for Ni (a ferromagnet with high T_C) is inconceivable, this possibility is completely ruled out. Another likely explanation is that some other type of interactions present in Ni wipes out the ISR 3D Heisenberg critical behavior within the part of the critical region covered in the present experiments, i.e., $3.0 \times 10^{-4} \leq |\epsilon| \leq 3.0 \times 10^{-2}$ (Tables I and II) and outside the critical regime the mean-field behavior takes over. We contend that these interactions are nothing but the *isotropic* long-range (ILR) *exchange* interactions of the form $-(J_\infty/r^{d+\sigma})\vec{S}_0 \cdot \vec{S}_r$ [where $0 < \sigma < 2$, $\sigma < (2 - \eta_{ISR})$; η_{ISR} is the correlation function critical exponent corresponding to the ISR 3D Heisenberg fixed point and $d < 2\sigma$] which render ISR 3D Heisenberg fixed point unstable and lead to a *crossover*³² to the ILR fixed point which is characterized by exponent values that are ISR 3D Heisenberg-like but shifted *towards* MF values [cf. observation (i) above]. For instance, if $\sigma = 1.91$, one obtains the values for the ILR fixed point critical exponents $\beta = 0.390$, $\gamma = 1.341$, and $\delta = 4.44$ from the expression for γ_{ILR} given in Ref. 32 and the scaling relations⁴ that are fairly close to the asymptotic values determined by us in this work (Table III). The long-range nature of exchange interactions in Ni is further supported by the result of spin-wave studies on Ni, that the range of the exchange interactions in Ni extends well beyond³³ the fourth nearest-neighbor distance. In this context, it is interesting to note that a d -dimensional spin system with isotropic long-range exchange interactions of the form given above exhibits the mean-field (or, more exactly, Gaussian) behavior³² in the other extreme case when $d > 2\sigma$ and $\sigma \neq 2$. At this stage, it should be emphasized that the present results cannot rule out the

existence of another crossover from an ILR fixed point to an IDL fixed point as $|\epsilon| \rightarrow 0$. If such a crossover indeed occurs, the problems associated with the rounding of transition at T_C , usually encountered³⁴ for $|\epsilon| < 10^{-4}$, would preclude its observation.

The lower value of the ratio $\mu(0)h_0/k_B T_C$ [observation (iii) above] implies that an *average effective* elementary moment (μ_{eff}) involved in the FM-PM phase transition has a value higher^{4,7,8,13} than $\mu(0)$ (moment per Ni atom at 0 K). If the value of this ratio, like those of exponents β and γ , lies between the 3D ISR Heisenberg and MF values, the concentration of such *effective* moments, $c = \mu(0)/\mu_{\text{eff}}$, should be around 80%. Thus, not all the moments but only $\approx 80\%$ of them actually participate in the magnetic order-disorder transition at T_C . This inference is in consonance with the existence of substantial short-range magnetic order at temperatures near T_C in Ni as revealed by the theoretical analysis^{35,36} of the spin- and angle-resolved ultraviolet photoemission data.³⁷

The validity of the Widom scaling relation between the critical exponents β , γ , and δ demands that the magnetic polarization data taken in the ACR should satisfy the scaling equation of state (SES)

$$m = f_{\pm}(h), \quad (12)$$

where plus and minus signs refer to temperatures above and below T_C , and $m \equiv J/|\epsilon|^\beta$ and $h \equiv \mu_0 H/|\epsilon|^{\beta+\gamma}$ are the scaled magnetic polarization and scaled field, respectively. Equation (12) implies that m as a function of h falls on two universal curves: $f_-(h)$ for $\epsilon < 0$ and $f_+(h)$ for $\epsilon > 0$. A typical plot of $\ln m$ against $\ln h$ depicted in Fig. 12 demonstrates that the magnetic polarization data do indeed obey the SES of the form given by Eq. (12).

About a decade ago, Souletie and Tholence³⁸ showed that the susceptibility χ_0 of crystalline Ni varies with temperature in accordance with the *generalized* Curie-Weiss law,³⁹ i.e.,

$$\chi_0(T) = A_\chi t^{-1} |\tilde{\epsilon}|^{-\gamma} + B_\chi, \quad (13)$$

where the Curie constant $C = A_\chi T_C$, $t = T/T_C$, $\tilde{\epsilon} = (T - T_C)/T$, and B_χ is a constant, over a wide temperature range which extends from T_C to $3T_C$. Note that these authors found it necessary to include the con-

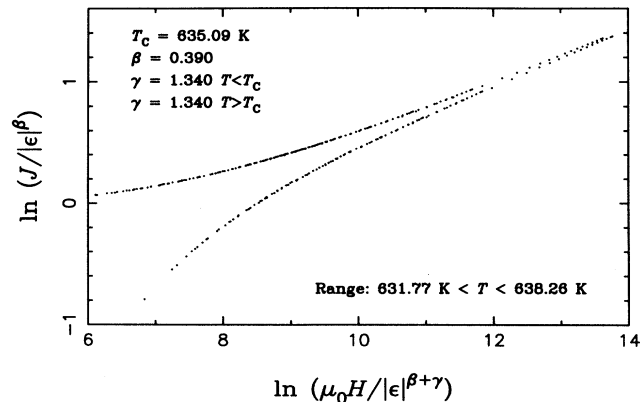


FIG. 12. Scaling plot for the Ni sample No. 3.

stant term B_χ in order to significantly improve agreement between the variation of χ_0 with T predicted by the first term in Eq. (13) and the observed $\chi_0(T)$. Recently, Kaul⁸ provided a theoretical basis for the first term in Eq. (13) and calculated both nonanalytic and analytic corrections, arising from nonlinear (NL) irrelevant scaling fields and NL relevant scaling fields, respectively, to this power law within the framework of RG theories.^{9,10} With only the leading correction terms included, his expression for $\chi_0(T)$ reads as⁸

$$\chi_0(T) = \tilde{A}_\chi t^{-1} |\tilde{\epsilon}|^{-\gamma} (1 + \tilde{a}_{\chi_1} |\tilde{\epsilon}|^\Delta + \tilde{a}_{\chi_2} \tilde{\epsilon}). \quad (14)$$

We have attempted a range-of-fit analysis of the $\chi_0^{-1}(T)$ data based on Eqs. (13) and (14) with the following result. (i) Equation (14) provides a decidedly better fit to the $\chi_0^{-1}(T)$ data than Eq. (13) regardless of the temperature range chosen for the fit. (ii) A nonanalytic correction term [i.e., the second term in Eq. (14)] dominates over the analytic one [third term in Eq. (14)] in the ACR [where Eq. (14) with $\tilde{a}_{\chi_2} = 0$ and Eq. (6) yield identical results and provide equally good fits to the $\chi_0^{-1}(T)$ data] but the reverse is true for $T \gg T_C$, as expected. (iii) Equation (14) with $\tilde{a}_{\chi_1} = 0$ provides a good overall fit (solid curve in Fig. 13) to the $\chi_0^{-1}(T)$ data over a wide temperature range $T_C \leq T \leq 1.4T_C$ which is *better* than that obtained based on Eq. (13) in the same temperature range (cf. χ^2 values in Table IV). (iv) Unlike \tilde{a}_{χ_2} , B_χ is extremely sensitive to the temperature range chosen for the fit. (v) In the entire temperature range covered in the present experiments, the fit based on Eq. (14) with $\tilde{a}_{\chi_1} = 0$ [Eq. (13)] yields a value for the critical exponent γ which is nearly the same as the *asymptotic (effective)* one; cf. Tables II and IV. Unlike the authors of Ref. 38, we consider this agreement as *fortuitous* because these fits exhibit systematic deviations from the data in the ACR where the nonanalytic term [i.e., the term $\tilde{a}_{\chi_1} |\tilde{\epsilon}|^\Delta$ in Eq. (14) or $a_\chi^+ \epsilon^\Delta$ in Eq. (6)] becomes important. Moreover, the Curie constant, defined as $C = A_\chi T_C$ in

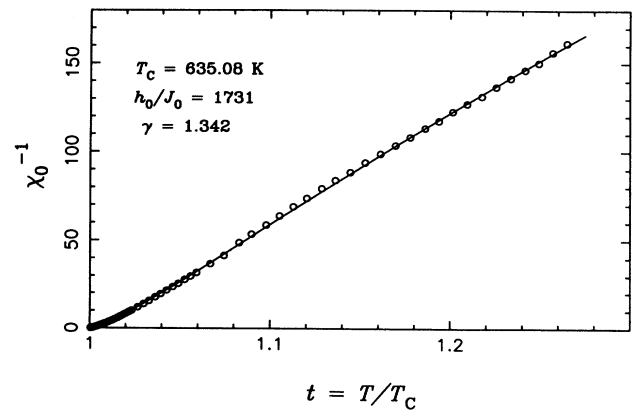


FIG. 13. Temperature dependence of inverse initial susceptibility for the Ni sample No. 3 over the entire temperature range covered in the present experiments. The solid curve through the data points denotes the best least-squares fit based on Eq. (14) with $\tilde{a}_{\chi_1} = 0$ and the parameter values given in Table IV.

TABLE IV. Parameter values for the fits to the $\chi_0^{-1}(T)$ data based on Eq. (14) with $\tilde{a}_{\chi_1} = 0$ and Eq. (13) of the text. $\chi^2 = [1/(N - N_p)] \sum_i [1 - \{Y_i(\text{calc})/Y_i(\text{expt})\}]^2$ where N and N_p denote the total number of data points and fitting parameters, respectively. Abbreviation: PW = present work.

Sample No.	Ref.	Fit to	Fit range		T_C^+ (K)	γ	C (K)	\tilde{a}_{χ_2}	B_χ (10^{-4})	q_c μ_B	q_c/q_s	χ^2 (10^{-1})
			t_{\min}	t_{\max}								
1	PW	Eq. (13)	1.00	1.40	635.54(3)	1.310(10)	0.0354(15)		7.05(55)	0.69(3)	1.15(5)	12.93
	PW	Eq. (14)	1.00	1.40	635.53(3)	1.340(10)	0.0290(15)	1.6(4)		0.59(3)	0.98(5)	12.80
2	PW	Eq. (13)	1.00	1.27	634.66(3)	1.305(10)	0.0353(14)		14.44(56)	0.69(3)	1.15(5)	10.83
	PW	Eq. (14)	1.00	1.27	634.64(2)	1.352(10)	0.0286(14)	2.5(4)		0.58(3)	0.97(5)	10.61
3	PW	Eq. (13)	1.00	1.26	635.09(3)	1.300(10)	0.0354(15)		18.94(56)	0.69(3)	1.15(5)	7.02
	PW	Eq. (14)	1.00	1.26	635.08(2)	1.342(10)	0.0292(15)	2.8(4)		0.59(3)	0.98(5)	6.84
4	PW	Eq. (13)	1.00	1.26	634.24(3)	1.310(10)	0.0353(14)		6.44(60)	0.69(3)	1.15(5)	10.94
	PW	Eq. (14)	1.00	1.26	634.23(2)	1.340(10)	0.0297(15)	1.5(5)		0.60(3)	1.00(5)	9.11
Ni	28	Eq. (13)	1.00	1.12	627.275	1.309(2)	0.0320		2.72	0.639	1.04	
	28	Eq. (13)	1.04	2.90	627.275	1.345(2)	0.0320		2.72	0.639	1.04	

Eq. (13) and $C = \tilde{A}_\chi T_C$ in Eq. (14), permits a calculation of the moment per Ni atom in the PM state, q_C , through the relation $p_{\text{eff}}^2 = (2.829)^2 (CA/\rho) = q_C(q_C + 2)$, where p_{eff} is the effective paramagnetic moment, A is the atomic weight, and ρ is the density. The values of q_C , so computed, and the ratio q_c/q_s [where q_s is the same as $\mu(0)$] are listed in Table IV. In the spirit of the Rhodes-Wohlfarth plot,⁴⁰ a value of the ratio q_c/q_s close to unity implies that the itinerant character of the magnetic electrons in Ni cannot be assessed unambiguously on the basis of the value of q_c/q_s ratio alone. Alternatively, a supporting evidence is needed to clarify the issue.

V. SUMMARY AND CONCLUSIONS

An elaborate analysis of high-precision bulk magnetic polarization data taken in the critical region near the FM-PM phase transition on polycrystalline Ni samples of four different shapes permits an accurate determination of the asymptotic critical exponents, the universal amplitude ratios, and the leading correction-to-scaling amplitudes. The presently determined values of the asymptotic critical exponents β , γ , and δ as well as the ratio $J_0/J_S(0)$ are close to those predicted by the RG calculations for a 3D isotropic short-range Heisenberg ferromagnet but shifted towards the mean-field values. In our opinion, such a shift in the exponent and amplitude ratio values, far from being a signature of the influence of isotropic long-range dipolar interactions on the critical behavior, indicates a *crossover* to the fixed point corresponding to

the *isotropic long-range* exchange interactions.

From the value of the ratio $\mu(0)h_0/k_B T_C$, we infer that only about 80% of the moments in Ni actually participate in the FM-PM phase transition. The other important observations include the following: (i) The exponents β , γ , and δ obey the Widom scaling relation $\beta\delta = \beta + \gamma$, and the magnetic polarization data, taken in the asymptotic critical region (ACR), satisfy the scaling equation-of-state characteristic of second-order phase transition, (ii) a nonanalytic correction term, originating from the nonlinear irrelevant scaling fields, dominates over the analytic one, arising on account of the nonlinear relevant scaling fields, in the ACR but the reverse is true for $T \gg T_C$, (iii) the functional dependence of the initial susceptibility on temperature in a wide temperature range $T_C \leq T \leq 1.4T_C$ is better described by Eq. (14) with $\tilde{a}_{\chi_1} = 0$ than by Eq. (13) and the atomic moment in the paramagnetic state can be accurately determined from the Curie constant, $C = \tilde{A}_\chi T_C$, and (iv) the shape anisotropy has no discernible effect on the low-field deviations in the modified Arrott plot.

ACKNOWLEDGMENTS

One of us (S.N.K.) would like to acknowledge the warm hospitality extended to him at the Max-Planck-Institute, Stuttgart, and thank the Max-Planck-Society for financial assistance. The authors thank Professor M. Föhnle for fruitful discussions.

* On leave from the School of Physics, University of Hyderabad, Central University P.O., Hyderabad-500134, Andhra Pradesh, India.

† Author to whom all correspondence should be sent at the above address.

¹ R.M. Suter and C. Hohenemser, J. Appl. Phys. **50**, 1814 (1979).

² C. Hohenemser, N. Rosov, and A. Kleinhammer, Hyperfine Interact. **49**, 267 (1989).

³ J.C. Le Guillou and J. Zinn-Justin, Phys. Rev. B **21**, 3976

- (1980); S.G. Gorishny, S.A. Larin, and F.V. Trachov, *Phys. Lett.* **101A**, 120 (1984); C. Bagnuls and C. Bervillier, *Phys. Rev. B* **32**, 7209 (1985).
- ⁴ S.N. Kaul, *J. Magn. Magn. Mater.* **53**, 5 (1985), and references cited therein.
- ⁵ S.N. Kaul, *Phys. Rev. B* **38**, 9178 (1988).
- ⁶ S.N. Kaul and M. Sambasiva Rao, *Phys. Rev. B* **43**, 11 240 (1991); *J. Phys. Condens. Matter* **6**, 7403 (1994).
- ⁷ M. Sambasiva Rao and S.N. Kaul, *J. Magn. Magn. Mater.* (to be published).
- ⁸ S.N. Kaul, *Phase Transitions* **47**, 23 (1994); S.N. Kaul and Ch.V. Mohan, *Phys. Rev. B* **50**, 6157 (1994).
- ⁹ F.J. Wegner, *Phys. Rev. B* **5**, 4529 (1972); M.E. Fisher, *Rev. Mod. Phys.* **46**, 597 (1974).
- ¹⁰ A. Aharony and G. Ahlers, *Phys. Rev. Lett.* **44**, 782 (1980).
- ¹¹ R. Reisser, M. Fähnle, and H. Kronmüller, *J. Magn. Magn. Mater.* **75**, 45 (1988).
- ¹² M. Seeger and H. Kronmüller, *J. Magn. Magn. Mater.* **78**, 393 (1989); M. Seeger, H. Kronmüller, and H.J. Blythe, *ibid.* **139**, 312 (1995).
- ¹³ R. Reisser, M. Fähnle, and H. Kronmüller, *J. Magn. Magn. Mater.* **97**, 83 (1991); R. Reisser and H. Kronmüller, *ibid.* **98**, 273 (1991); R. Reisser and H. Kronmüller, *ibid.* **128**, 341 (1993).
- ¹⁴ R. Reisser, M. Seeger, M. Fähnle, and H. Kronmüller, *J. Magn. Magn. Mater.* **110**, 32 (1992); R. Reisser, M. Seeger, and H. Kronmüller, *ibid.* **128**, 321 (1993).
- ¹⁵ W.-U. Kellner, M. Fähnle, H. Kronmüller, and S.N. Kaul, *Phys. Status Solidi B* **144**, 397 (1987).
- ¹⁶ J.S. Kouvel and M.E. Fisher, *Phys. Rev.* **136**, A1626 (1964).
- ¹⁷ D.S. Greywall and G. Ahlers, *Phys. Rev. Lett.* **28**, 1251 (1972); D. Balzarini and K. Ohrn, *ibid.* **29**, 840 (1972).
- ¹⁸ J.S. Kouvel and J.B. Comley, *Phys. Rev. Lett.* **20**, 1237 (1968).
- ¹⁹ N. Stüsser, M.Th. Rekveldt, and T. Spruijt, *Phys. Rev. B* **33**, 6423 (1986).
- ²⁰ V. Privman, P.C. Hohenberg, and A. Aharony, in *Phase Transitions and Critical Phenomena*, edited by C. Domb and J.L. Lebowitz (Academic, New York, 1991), Vol. 14, p. 1.
- ²¹ A. Arrott and J.E. Noakes, *Phys. Rev. Lett.* **19**, 786 (1967).
- ²² R.C. Reno and C. Hohenemser, *Phys. Rev. Lett.* **25**, 1007 (1970).
- ²³ C. Hohenemser, T.A. Kachnowski, and T.K. Bergstresser, *Phys. Rev. B* **13**, 3154 (1976).
- ²⁴ T.A. Kachnowski, R.M. Suter, A.M. Gottlieb, and C. Hohenemser, *Phys. Rev. B* **14**, 5022 (1976).
- ²⁵ A. Aharony and M.E. Fisher, *Phys. Rev. B* **8**, 3323 (1973).
- ²⁶ M.E. Fisher and A. Aharony, *Phys. Rev. Lett.* **30**, 559 (1973).
- ²⁷ A.D. Bruce and A. Aharony, *Phys. Rev. B* **10**, 2078 (1974).
- ²⁸ A.D. Bruce, J.M. Kosterlitz, and D.R. Nelson, *J. Phys. C* **9**, 825 (1976); T. Nattermann and S. Trimper, *ibid.* **9**, 2589 (1976); A.D. Bruce, *ibid.* **10**, 419 (1977).
- ²⁹ E. Frey and F. Schwabl, *Phys. Rev. B* **43**, 833 (1991).
- ³⁰ N. Menyuk, K. Dwight, and T.B. Reed, *Phys. Rev. B* **3**, 1689 (1971).
- ³¹ A. Kornblit, G. Ahlers, and E. Buehler, *Phys. Rev. B* **17**, 282 (1978).
- ³² M.E. Fisher, S.K. Ma, and B.G. Nickel, *Phys. Rev. Lett.* **29**, 917 (1972); A. Aharony, in *Phase Transitions and Critical Phenomena*, edited by C. Domb and M.S. Green (Academic, New York, 1976), Vol. 6, p. 357.
- ³³ S.N. Kaul, *Phys. Rev. B* **27**, 5761 (1983).
- ³⁴ G. Ahlers and A. Kornblit, *Phys. Rev. B* **12**, 1938 (1975).
- ³⁵ V. Korenman and R.E. Prange, *Phys. Rev. Lett.* **53**, 186 (1984).
- ³⁶ E.M. Haines, V. Heine, and A. Ziegler, *J. Phys. F* **16**, 1343 (1986).
- ³⁷ E. Kisker, in *Polarized Electrons in Surface Physics*, edited by R. Feder (World Scientific, Singapore, 1985), p. 513; see also R. Clauber and R. Feder, in *ibid.*, p. 565.
- ³⁸ J. Souletie and J.L. Tholence, *Solid State Commun.* **48**, 407 (1983).
- ³⁹ A.S. Arrott, *Phys. Rev. B* **31**, 2851 (1985).
- ⁴⁰ E.P. Wohlfarth, *J. Magn. Magn. Mater.* **7**, 113 (1978).